Particles II
Access the latest eBook →

Impact on Biological Systems and the Environment

11 Advanced Optical Metrology

Particles II

EVIDENT
OLYMPUS

WILEY

This eBook is dedicated to the research of Professor David Wertheim.
In collaboration with various groups, Professor Wertheim uses confocal microscopy to analyse the impact of different types of particles on human health and the environment, with a focus on human health-hazardous particles detected with solid-state nuclear track detectors (SSNTD). Download for free, today.

EVIDENT
OLYMPUS

WILEY

Peptide-Based Coacervate-Core Vesicles with Semipermeable Membranes

Manzar Abbas,* Jack O. Law, Sushma N. Grellscheid, Wilhelm T. S. Huck, and Evan Spruijt*

Coacervates droplets have long been considered as potential protocells to mimic living cells. However, these droplets lack a membrane and are prone to coalescence, limiting their ability to survive, interact, and organize into higher-order assemblies. This work shows that tyrosine-rich peptide conjugates can undergo liquid–liquid phase separation in a well-defined pH window and transform into stable membrane-enclosed protocells by enzymatic oxidation and cross-linking at the liquid–liquid interface. The oxidation of the tyrosine-rich peptides into dityrosine creates a semipermeable, flexible membrane around the coacervates with tunable thickness, which displays strong intrinsic fluorescence, and stabilizes the coacervate protocells against coalescence. The membranes have an effective molecular weight cut-off of 2.5 kDa, as determined from the partitioning of small dyes and labeled peptides, RNA, and polymers into the membrane-enclosed coacervate protocells. Flicker spectroscopy reveals a membrane bending rigidity of only $0.1k_BT$, which is substantially lower than phospholipid bilayers despite a larger membrane thickness. Finally, it is shown that enzymes can be stably encapsulated inside the protocells and be supplied with substrates from outside, which opens the way for these membrane-bound compartments to be used as molecularly crowded artificial cells capable of communication or as a vehicle for drug delivery.

1. Introduction

Compartmentalization is a hallmark of life and is a central goal in current efforts to construct artificial cells.[1] Different types of compartments, including liposomes, proteinosomes, polymersomes, and coacervates, have been studied to obtain insights into the role of compartmentalization on biomolecules and biochemical reaction networks commonly found in living cells.[2] However, these compartments are unable to mimic all the functional characteristics of living cells, which include a high internal concentration of biomolecules, a selective membrane and an ability to interact with other cells.

Coacervate droplets are one type of cell-like compartment, which are formed spontaneously through liquid–liquid phase separation (LLPS) of RNA, peptides or small molecules, driven by a multitude of non-covalent interactions.[3] The physical properties of coacervates depend on the structure–function relationships of their constituting building blocks. In general, they contain high concentrations of peptides or RNA, which mimics the physicochemical environment inside living cells.[4] However, the lack of a membrane, which typically leads to rapid coalescence, poses a challenge to their stability. Moreover, the absence of a barrier means that selectivity in the uptake of nutrients, and removal of waste while retaining useful products, is difficult.[3,5] Lipid-based membrane-bound compartments, of which liposomes are the best-known example, are also commonly studied as protocells models, but they usually contain low concentrations of solutes inside compared to the concentration of biomolecules in living cells, or they risk bursting when the high osmotic pressure is not carefully balanced.[6]

Therefore, researchers have sought to combine these two worlds and construct hybrid protocells with a coacervate-based interior and a membrane-based casing. The membrane can either be formed directly around a coacervate droplet, which acts as a template, or the membrane can enclose one or multiple coacervate droplets dispersed in solution. Using the template approach, coacervates with membranes made of various phospholipids and fatty acids have been reported. Typically, two oppositely charged components were mixed to form complex

M. Abbas, W. T. S. Huck, E. Spruijt
Institute for Molecules and Materials
Radboud University
Heyendaalseweg 135, Nijmegen 6525 AJ, The Netherlands
E-mail: m.abbas@science.ru.nl; e.spruijt@science.ru.nl
J. O. Law, S. N. Grellscheid
Computational Biology Unit
University of Bergen
Bergen 5020, Norway
S. N. Grellscheid
Department of Biosciences
Durham University
Durham DH1 3LE, UK

**ADVANCED
SCIENCE NEWS**
www.advancedsciencenews.com

**ADVANCED
MATERIALS**
www.advmat.de

coacervates in the first step, and lipids or fatty acids were assembled into a bilayer around the coacervates in a second step.[4b,7] The interfacial self-assembly of block copolymers outside coacervates[8] and assembly of polyoxometalate layers have also been reported.[9] Both of these dramatically increase the stability of coacervates, but are considered to be more distant from the origins of life.

Recently, coacervates have also been encapsulated inside liposomes through several approaches. Deng et al. used a microfluidic platform to separate the components of a complex coacervate in parallel flows and encapsulate them in a liposome.[10] Upon encapsulation, the components were mixed and coacervate droplets nucleated inside the liposomes. They showed that this approach yielded monodisperse coacervate organelles and that the coacervates were able to localize the aptamer product of a cell-free transcription reaction. Moreover, this platform could be used to create liposomes containing coacervates that formed in response to temperature changes,[10] and ionic strength changes applied by shrinking.[11] Deshpande et al. used a slightly different microfluidic platform to encapsulate one of the coacervate-forming components together with a pore-forming protein inside liposomes.[12] Coacervation was then induced by influx of small nucleotides (ATP) through the membrane pores. The nucleation and coalescence of coacervate droplets inside liposomes could be monitored, and it was shown that the coacervate could act to localize an enzymatic reaction. Finally, Last et al.[13] and Love et al.[14] encapsulated a mixture of oppositely charged molecules just outside the phase-separated region in a liposome, and induced coacervation by changing the pH of the surrounding solution.

However, in all these "hybrid" protocells the membranes are made of different building blocks than the coacervates, and they have limited permeability. From a primitive cell perspective, one of the simplest scenarios is a single species that is able to both condense into droplets and form a membrane layer that offers stability and selectivity, for example through crosslinking. Moreover, by forming a membrane directly from the coacervate forming molecules, it may be possible to alter the membrane thickness or permeability, and by extension other membrane properties like stiffness, by tuning the crosslinking extent.

Here, we show that tyrosine-rich short peptide derivatives are indeed capable of forming hybrid protocells with a coacervate core and a flexible, semipermeable membrane that provides stability to the coacervates, and enables size-selective uptake of molecules from the surrounding solution. Inspired by our recently reported short-peptide synthon for phase separation,[15] we designed a series of tyrosine-rich peptide conjugates that show a remarkable variety of phase transitions, depending on the molecular characteristics of the spacer connecting the tyrosine-rich stickers. We observed needle-like fibers nucleated from a central core, fractal-like structures of agglomerated nanoparticles, and LLPS droplets that could undergo fusion and wetting. Unlike previously reported short peptide derivatives, the phase separation of these tyrosine-rich conjugates can be controlled in a well-defined pH window, which makes them interesting protocell candidates that could form at specific locations in response to pH changes. Moreover, the tyrosine residues enable oxidative crosslinking, which can be used to

stabilize the coacervates from coalescence. By using an enzyme that is only active outside the coacervates, the oxidation results in a relatively thin membrane-like layer with a significant flexibility (surface tension 45 nN m^{-1}, bending rigidity $0.1k_BT$), that acts as a protective membrane around the dense coacervate core, and keeps the coacervate protocells stable for more than a month. The membranes are permeable to small molecules and have a molecular weight cut-off of 2.5 kDa. Because the core of the vesicles is a peptide-based coacervate, small molecules that can pass the membrane can be concentrated more than tenfold, while large molecules are effectively excluded, making these hybrid coacervate compartments suitable for storage and triggered release of nutrients or drugs in crowded biomolecular environments.

2. Results and Discussion

2.1. Molecular Design of Peptide Conjugates for Crosslinkable Coacervates

We previously found that short peptide conjugates with two hydrophobic dipeptide stickers connected by a polar, flexible spacer are able to condense into liquid droplets at neutral pH and sub-millimolar concentrations.[15] Here, we aim to create a semipermeable membrane around these droplets in order to improve their stability and enable a size-selective uptake of molecules by introducing tyrosine residues in the dipeptide stickers. Tyrosines commonly occur in the intrinsically disordered regions of proteins that are known to phase separate,[16] and they can interact through cation–π and π–π interactions. The presence of a phenol group is expected to lower the hydrophobicity of the stickers compared to diphenylalanine and lead to an increased solubility.[17] However, by introducing a single tyrosine in each dipeptide sticker, we expect the conjugates to still phase separate, as stickers with a single leucine (FL and LF), which have comparable hydrophobicity, and also stickers with a double leucine (LL) were previously found to phase separate.[15] Because the spacer is known to have a more subtle effect on the final appearance and properties of the condensates, we first investigated the phase behavior of a series of peptide conjugates with tyrosine-containing stickers and spacers with different polarities.

We designed and synthesized five small peptide-based sticker–spacer–sticker molecules with different spacers, as shown in **Figure 1**a and Table S1, Supporting Information. All five peptide conjugates were soluble in water at pH below 6.5, and initially underwent LLPS (self-coacervation) upon increasing the pH to 7 or above. The coacervates further coalesced or agglomerated into various types of structures (droplets, urchin-like microstructures or fractals) depending on the spacer. The peptide derivative with a spacer of 2,2′-thiobis(ethylamine) (TBEA) and two tyrosine-phenylalanine (YF) stickers (abbreviated as YFsFY) formed clear liquid coacervates (Figure 1b) that fused readily (Figure S1 and Video S1, Supporting Information). Changing the position of the amino acid residues in the sticker did not affect the self-coacervation of these derivatives (Figure 1c), similar to previous studies with stickers containing leucines.[15] When we replaced the TBEA

ADVANCED
SCIENCE NEWS
www.advancedsciencenews.com

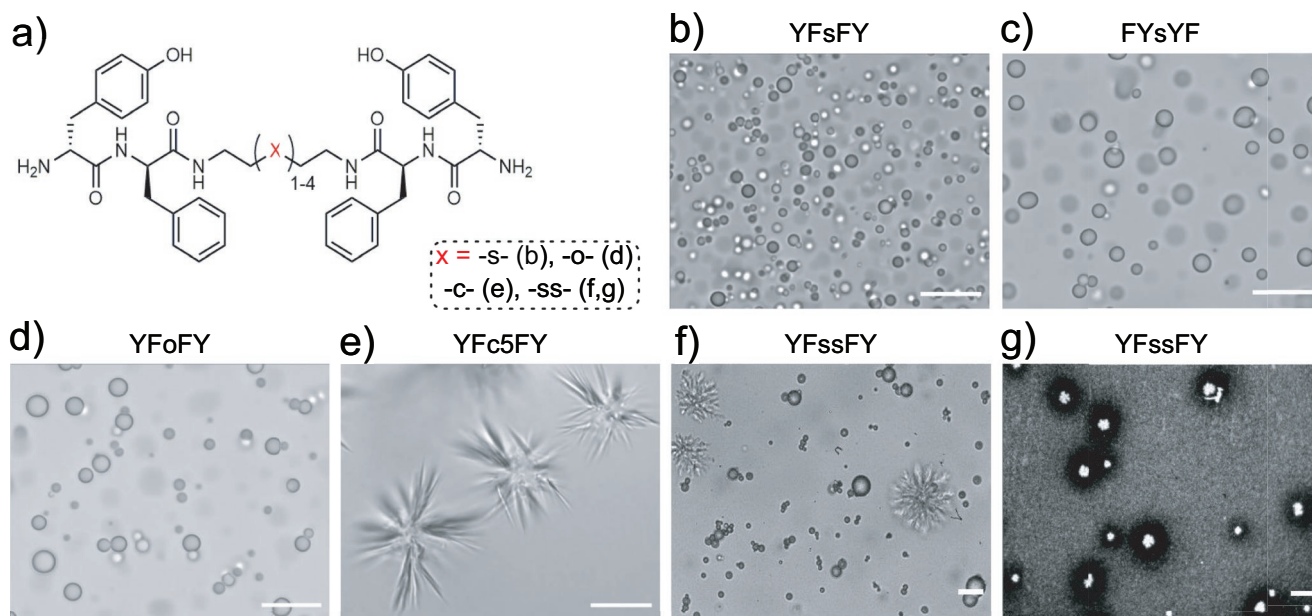ADVANCED
MATERIALS
www.advmat.de

Figure 1. a) General chemical structure of designed small peptide-based molecules with four different spacers. Full structures are shown in Table S1, Supporting Information. b–f) Optical microscopy images of the coacervates formed from the derivatives depicted in (a): b) 2 mg mL^{-1} YFsFY, c) 2 mg mL^{-1} FYsYF, d) 2 mg mL^{-1} YFoFY, e) 2 mg mL^{-1} YFc5FY, and f) 2 mg mL^{-1} YFssFY. g) Dark-field image of fractal microstructures of YFssFY. The scale bar in all images represents 10 µm.

spacer with 2,2′-oxydiethylamine dihydrochloride (ODEA), the physical appearance of coacervates remained the same, which may be attributed to the similar polarity[15] of the two spacers (Figure 1d).

Contrary to the coacervates of short peptide conjugates with polar spacers, the coacervates of more apolar spacers, like pentane-1,5-diamine carbonate (cadaverine), showed a rapid liquid-to-solid transition (less than 1 min), resulting in star-shaped needle-like microstructures with a striking resemblance to the "sea urchin" structures observed for FUS droplets (Figure 1e, and Figure S2a–d and Video S2, Supporting Information).[18] Finally, conjugates with a cystamine spacer formed small gel-like coacervates upon increasing the pH (Figure 1f). Interestingly, these gel-like coacervates did not fuse as readily as the coacervates in Figure 1c,d, but slowly agglomerated into fractal microstructures around sparse nuclei through collisions. The collision-induced growth leaves a clear depletion zone around the fractal microstructures which grows as $t^{1/2}$ (Figure S3 and Video S3, Supporting Information), and can be visualized by dark-field microscopy (Figure 1g). It is not clear why nucleation of these fractals only occurs in a few sparsely distributed locations, but we speculate that exposure to air can create phenoxy radicals at the surface of certain coacervates, which react with other tyrosines upon collision. Interestingly, the coacervates within the fractal microstructures remain solvated and can still take up selected dye molecules, resulting in highly fluorescent stars (Figure S4, Supporting Information).

2.2. pH Window for Stable Coacervates

Of the designs shown in Figure 1, we selected the YFsFY conjugate with a 2,2′-thiobis(ethylamine) (TBEA) spacer to create

coacervate protocells with a semipermeable stabilizing membrane by oxidation. Because the phenolic side group of tyrosine has a p$K_a \approx 10.5$, we first investigated if these coacervates could also be dissolved at high pH. For complex coacervates, it has been shown that they are only stable when the two components are charged: they can be dissolved either by deprotonating the cationic species or by protonating the anionic species, since the phase separation is driven by charge interaction.[19] However, for simple coacervates, where phase separation is driven by a combination of cation–π and π–π interactions, it is not clear if (de)protonation could disrupt these interactions sufficiently to destabilize the coacervates (**Figure 2**a).

Therefore, we investigated the phase behavior of YFsFY as a function of pH by combined turbidity and microscopy measurements. Figure 2b shows that coacervates are formed in a specific pH window between 6.8 and 10.5. When the pH of an initially transparent solution (Figure 2c) was increased to 7 by using NaOH (1 M) or a Tris-buffer (100 × 10^{-3} M), coacervates emerged (Figure 2c) and the solution turned very turbid within seconds. As the pH was increased further, turbidity reached a maximum around pH 9 and decreased to baseline levels above pH 10.5. At that point, all coacervates had dissolved and the solution became transparent again (Figure 2c,d).[20] Note that the point at which coacervates dissolve is dependent on the concentration of the peptide-based conjugates and the salt concentration.[15,21] Without added salt, YFsFY dispersions were still turbid at pH 10.5 and coacervates could be observed (Figure S5a,b, Supporting Information).

To connect the pH-induced formation and dissolution of simple coacervates to changes in the molecular protonation state, we fitted the turbidity data to a model of a weak diprotic acid with two dissociation equilibria. When we plotted the relative amount of the intermediate, zwitterionic form, the
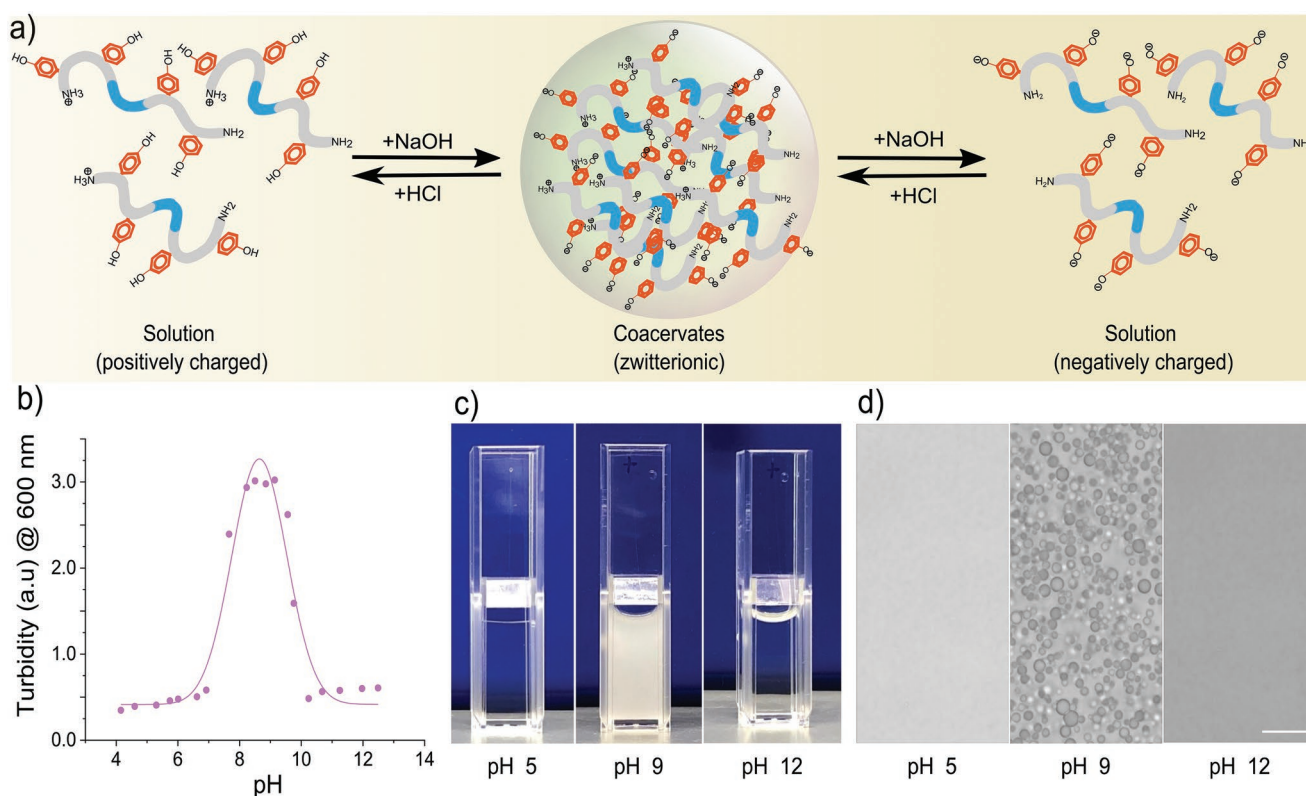
Figure 2. Simple coacervate formation in a pH window. a) Schematic illustration of YFsFY in solution at pH 4 (positively charged), in coacervates at pH 9 (zwitterionic form) and in solution at pH 12 (negatively charged). b) Turbidity of 1 mg mL^{-1} YFsFY as a function of pH with constant salt concentration of 65×10^{-3} M shows the formation of coacervates in a pH window between 7 and 10.5. The solid line is a fit of the turbidity data to a 2-pK_a model. c) Appearance of 2 mg mL^{-1} YFsFY solution at pH 5, 9, and 12. d) Bright-field optical microscopy of the samples in (c) shows the presence of coacervates at pH 9. The scale bar in (d) is 10 µm.

model with two pK_a values of 6.9 and 10.4, respectively, could capture the data surprisingly well (Figure 2b and Figure S5c, Supporting Information, for YFssFY). This suggests that only the zwitterionic species is able to form coacervates. The higher pK_a value of 10.4 found from our fit corresponds well with the expected pK_a of the tyrosine side group, indicating that deprotonation of the phenol can solubilize YFsFY and YFssFY coacervates. The lower pK_a value of 6.9 corresponds most likely to the protonation of the primary amines at the termini of the conjugates. This value is on the lower end of typical pK_a values for protein terminal amine groups,[22] which is most likely caused by the Born effect (dehydration) inside the relatively hydrophobic coacervates.

2.3. Oxidative Formation of Fluorescent Membranes around Coacervates: Coacervate-Core Vesicles

To create protective membranes around the peptide-based coacervate protocells, we used oxidative crosslinking of tyrosines to form dityrosine (**Figure 3**a), a process that occurs in nature under conditions of oxidative stress,[23] and has been used to create crosslinked networks in a variety of bioinspired structures and materials.[24] Tyrosine oxidation can be catalyzed by enzymes and UV light, typically leading to the formation of dopa, dityrosine, and melanin compounds, and has been

used to create nanofibers, peptidosomes, and photothermal sheets.[24a,c,25]

We used horseradish peroxidase (HRP) and hydrogen peroxide (H$_2$O$_2$) to convert tyrosine residues into dityrosines at the outer surface of YFsFY coacervates (Figure 3a). After the formation of coacervates, we added 2–10 µL H$_2$O$_2$ (1 M) to 100 µL of coacervates at pH 10–10.5, and subsequently 5–15 µL of freshly prepared HRP solution (5 mg mL^{-1}). We note that the pH used for oxidation differs from the pH at which maximum turbidity is reached (Figure 2b), because the HRP-catalyzed oxidation reaction requires the tyrosine residues to be mostly deprotonated. We confirmed that coacervates were not dissolved under the conditions selected for the oxidation reaction (Figure S5a,b, Supporting Information). The reaction mixture was kept at 4 °C for 24 h, because HRP has shown significant tyrosine oxidation activity at lower temperatures. After 24 h of oxidation, we examined the oxidized YFsFY coacervates by optical and fluorescence microscopy. We found that coacervate-core vesicles (CCVs) had been formed with a diameter ≈1–10 µm (Figure 3a and Figure S6a–e, Supporting Information), which showed strong fluorescence upon excitation at 315 nm, corresponding to the absorption maximum of dityrosine (Figure 3e). Interestingly, we did not observe any coalescence of CCVs, despite their sometimes very close packing (Figure 3c), which already suggests that the membranes are solid-like and capable of stabilizing the YFsFY coacervates. The solid nature of the
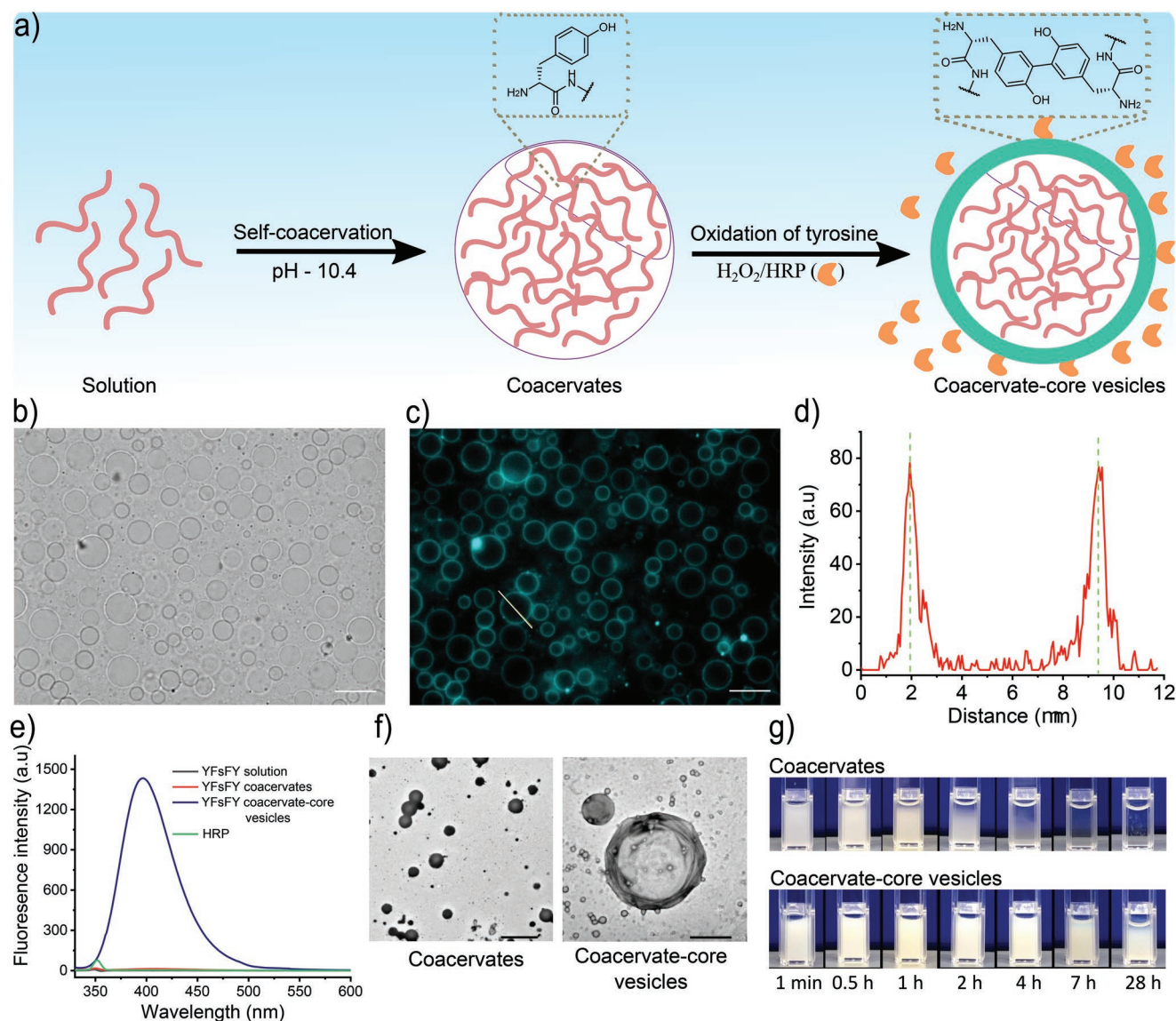
Figure 3. a) Schematic illustration of formation of CCVs. b) Bright-field and c) fluorescence microscopy of the CCVs formed after the oxidation of YFsFY coacervates (10 mg mL⁻¹). Scale bars indicate 10 μm. d) Intensity profile across a CCVs in (c). e) Fluorescence spectra of YFsFY coacervates before and after oxidation along with controls. f) Transmission electron microscopy images of coacervates (left) and CCVs (right); scale bars: 5 and 1 μm, respectively. g) Stability of CCVs in comparison with the coacervates without oxidizing agents (min = minutes and h = hours).

membrane was confirmed by photobleaching experiments (Figure S7, Supporting Information). Finally, the presence and stabilizing effect of the membrane could also be seen in transmission electron microscopy (TEM) images of the dehydrated CCVs. Unoxidized coacervates were dried into amorphous deposits (Figure 3f, left panel), while the oxidized samples did not spread out and retained their structure (Figure 3f, right panel). Similar CCVs could be formed from FYsYF coacervates (Figure S6f, Supporting Information), indicating that the order of amino acids in the stickers does not affect the crosslinking.

We analyzed the fluorescence of the CCVs by fluorescence spectroscopy and found an emission maximum at 405 nm (Figure 3e). Control samples with only HRP, with non-oxidized YFsFY dissolved at pH 6, and non-oxidized coacervates of YFsFY at pH 9 did not show any fluorescence signal at the

same excitation wavelength (Figure 3e). This confirms that the oxidation of YFsFY with H_2O_2/HRP results in the formation of dityrosines, which have strong intrinsic fluorescence. The HRP-catalyzed oxidation of tyrosines leads to formation of dopa, as well as dityrosines via tyrosyl radical rearrangement, as confirmed by matrix-assisted laser desorption/ionization time-of-flight (MALDI-TOF) mass spectrometry (Figure S8, Supporting Information). High-performance liquid chromatography (HPLC) and NMR analysis of CCVs collected by sedimentation, washed and dissolved in acetonitrile containing 1% v/v TFA showed that, besides dimers, oligomers with a broad distribution of sizes had formed (Figures S9 and S10, Supporting Information).

The thickness of the membranes was estimated from fluorescence microscopy images (Figure 3d) to be ≈800 nm,

ADVANCED
SCIENCE NEWS
www.advancedsciencenews.com

ADVANCED
MATERIALS
www.advmat.de

independent of the coacervate size. The thickness of the membrane can be tuned between roughly 300–900 nm by varying the concentrations of H_2O_2 and HRP as shown in Figure S6b–e, Supporting Information. In general, a lower coacervate concentration and a higher concentration of H_2O_2 and HRP lead to more rapid crosslinking and thinner membranes.

The fact that all CCVs formed under a certain set of conditions have a similar membrane thickness indicates that the membranes were formed by oxidation taking place at the interface of the coacervates, originating from the localization of HRP to the interface (Figure S11, Supporting Information). Radicals generated at the outer surface have a finite reactivity radius that is the same for all coacervates, since their internal peptide concentration is the same. Because of the low saturation concentration of YFsFY in the solution outside of the coacervates, only the radicals generated by enzymes present near the surface are able to induce crosslinking between YFsFY conjugates, which results in the formation of a dityrosine membrane.

Non-stabilized coacervate protocells undergo rapid coalescence, resulting in accelerated sedimentation and macroscopic separation of phases. A concentrated dispersion of micrometer-sized coacervates is therefore usually not stable for much longer than a few hours.[26] Adding a stabilizing membrane should prevent coalescence and wetting, and result in a significant increase in stability. We thus investigated the effect of dityrosine membranes on the stability of YFsFY coacervates by monitoring the appearance of a dispersion of oxidized coacervates in a cuvette. While untreated coacervates show rapid coalescence followed by sedimentation in ≈2 h, the vesicles formed after the oxidation of YFsFY sediment much slower, with a significant fraction of the coacervate-core vesicles still dispersed after 28 h (Figure 3g). Moreover, these vesicles retain their "identity" even after sedimentation, as they do not coalesce or spread on the cuvette bottom or side walls. They can be easily redispersed (Figure S12b, Supporting Information), and remain stable for more than 30 days (Figure S13, Supporting Information).

2.4. Membrane Permeability of Coacervate-Core Vesicles

Many stable membrane-bound compartments, including liposomes and polymersomes, have limited permeability for polar and charged nutrients. Proteinosomes[27] and colloidosomes[28] are notable exceptions, showing excellent stability and permeability to short oligonucleotides, peptides and even nanoparticles. We studied the permeability of coacervate-core vesicles formed by oxidation of YFsFY coacervates with a series of probe molecules with increasing molecular weight and varying charge.

Figure 4a–f shows fluorescence microscopy images of coacervate-core vesicles in the presence of ≈100 × 10⁻⁶ M of
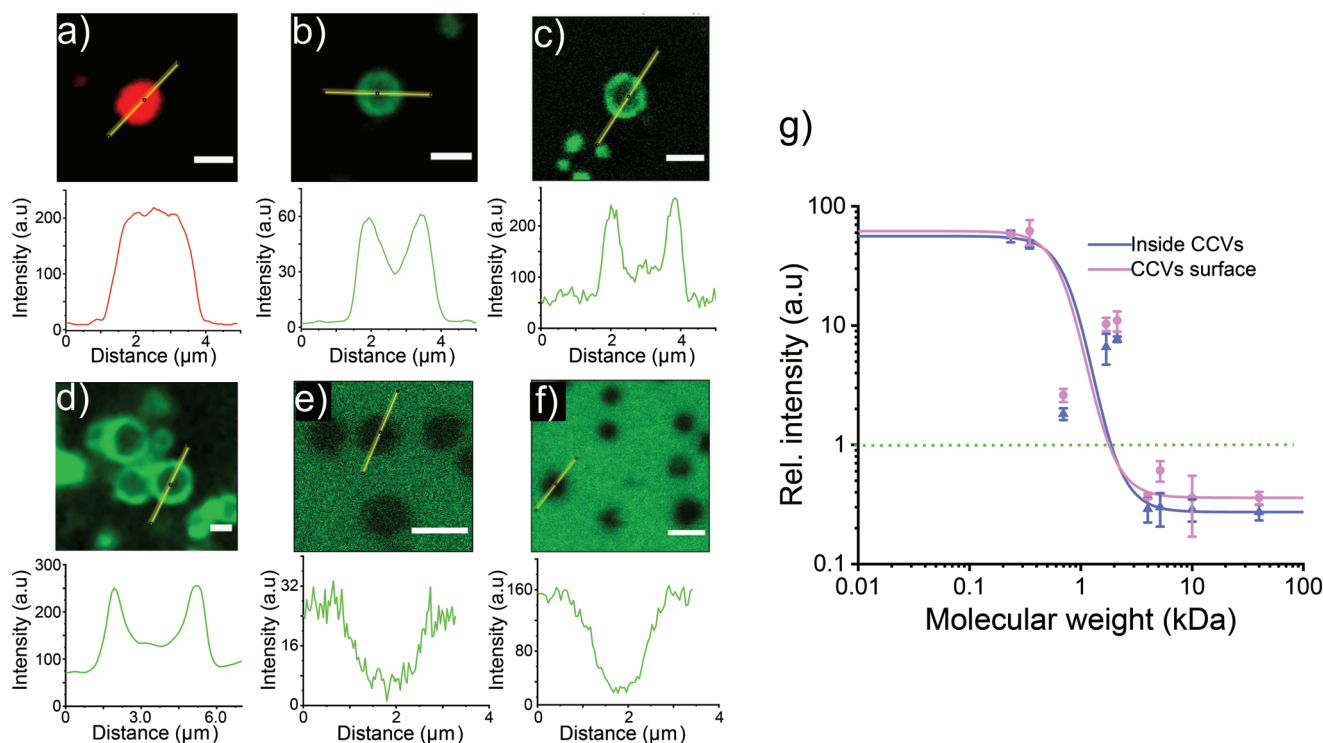

Figure 4. a–f) Permeability of coacervate-core vesicles with crosslinked dityrosine shells for probe of increasing molecular weight: a) resorufin, b) 4-amino fluorescein, c) FITC–GSH, d) FITC–K_{10}, e) FITC–dextran (4 kDa), and f) FITC–dextran (40 kDa). The upper panels are fluorescence microscopy images, lower panels intensity profiles across a vesicle. The scale bar in all images is 2 µm. g) Relative client concentration in the coacervate core and vesicle membrane as a function of molecular weight in kilodaltons ($n = 10$). The error bars represent the standard deviation over 10 CCVs. Images of neutral FITC–dextran (10 kDa), positively charged FAM-$(RRASL)_3$ and negatively charged ssDNA are shown in Figure S15, Supporting Information. The solid lines are fits of the data to a logistic function, from which a molecular weight cutoff (relative intensity < 1 shown by green dotted line) of 2.5 kDa was obtained.

fluorescently labeled probe molecules. Small molecular weight dyes and short peptides (up to 1 kDa) are able to cross the dityrosine membrane and end up being concentrated inside the vesicles, compared to the concentration of the solution outside. Zwitterionic dyes (aminofluorescein) and positively charged peptides (fluorescein isothiocyanate (FITC)–oligo-L-lysine (K_{10}) and FAM-$(RRASL)_3$) are preferentially accumulated at the membrane surface, or in the membrane layer, which we found carries a net negative charge at pH > 8.2 (Figure S14b, Supporting Information). However, these probes are also significantly concentrated in the coacervate core of the vesicles. Neutral dyes (resorufin) are more strongly taken up inside the core, although FITC–gluthathione (GSH) was found to be accumulated at the vesicle surface as well. When we use the comparatively bigger negatively charged DNA oligomers, we found that they were weakly excluded from the coacervate cores and the vesicle surface (Figure S15a, Supporting Information). Also larger neutral probe molecules were unable to permeate the membrane and were excluded from both the coacervate core and vesicle layer (Figure 4e,f), even after 24 h of incubation (Figure S16, Supporting Information). By plotting the apparent partitioning coefficients of all probe molecules in the coacervate core and the shell layer, as a function of their molecular weight, we found a molecular weight cut-off (where $K < 1$) of 2.5 kDa (Figure 4g).

2.5. Membrane Characteristics of Coacervate-Core Vesicles Enables Budding

The bending rigidity and surface tension of a membrane quantify the energy that is required to change the membrane curvature and increase the area, for example during shape deformations, endocytosis, tubulation, budding or division.[29] The intrinsic rigidity (bending modulus) stabilizes the membrane against fluctuations that result in local bending of the membrane, while the surface tension (mechanical membrane tension) acts within the membrane and stabilizes against deformations that result in stretching of the membrane.[30] Phospholipid-based bilayers exhibit a bending rigidity of the order of $25k_BT$,[29a,31] and a membrane tension between 100 nN/m and 2 mN m^{-1}, depending on the osmotic balance,[32] which enables thermal fluctuations to induce undulations in the shapes of GUVs that can be measured by microscopic contour analysis,[33] while energy-driven perturbations, usually mediated by enzymes, can easily lead to strong deformations, including tubulation and budding.[34]

We quantified the membrane characteristics of CCVs by flicker spectroscopy. Oxidized YFsFY vesicles show clearly measurable shape fluctuations despite their small size (**Figure 5**a and Video S4, Supporting Information). Frequency analysis of these fluctuations reveals a bending rigidity of $0.1k_BT$ and surface tension of 45 nN m^{-1} (Figure 5a), substantially lower than membranes composed of phospholipids, despite their larger thickness. This suggests that the dityrosine membranes can display large thermal shape fluctuations.

Interestingly, we found that these shape fluctuations can be further enhanced by adding a small amount of base to the oxidized CCVs to increase the pH further to 10.5. Figure 5b

shows snapshots of a vesicle displaying large amplitude and wavelength shape fluctuations, as a result of the mismatch between the membrane area and the preferred area of the coacervate core. The addition of base leads to partial dissolution (Figure 2b) and shrinkage of the coacervate core, while the membrane area is not decreased simultaneously. As a result, the vesicle adopts a shape with larger area to volume ratio than the original spherical shape, and, interestingly, this shape can fluctuate. Ultimately, these fluctuations can lead to the appearance of one or more buds on the membrane (Figure 5c and Video S5, Supporting Information), resembling budding in yeast. We did not observe the spontaneous abscission of the formed buds, but we note that shear forces or other forms of agitation could have caused the abscission in primitive cells made from peptide-based coacervates with membranes.[35]

2.6. External Nutrient Supply to Enzymes Stored in Coacervate-Core Vesicles

The assembly of a semipermeable membrane around these coacervates could provide a strategy to sequester and retain large functional molecules, such as enzymes. As a proof of principle, we encapsulated the enzyme beta-galactosidase (β-Gal) inside the shells and supplied it with a fluorogenic substrate in the outer solution (**Figure 6**a). We first mixed a low concentration of β-Gal (120 µg mL^{-1}) with the YFsFY pre-coacervate solution (5 mg mL^{-1}) at pH 6.5. Then, the pH was increased to 10.4 to induce coacervation and the tyrosine oxidizing mixture (H$_2$O$_2$ and HRP) was added and aged for 24 h. After membrane formation, the sample was centrifuged for 5 min at 4000 rcf, the supernatant was removed and the pellet of CCVs was washed with 20×10^{-3} M Tris- buffer pH 7.5, to remove nonencapsulated enzymes. The CCVs were resuspended in Milli-Q.

As the tyrosine oxidation occurs exclusively at the surface of the coacervates, active enzymes (β-Gal) that have been sequestered inside the coacervate core before the addition of H$_2$O$_2$ and HRP should be protected from oxidation. We confirmed that β-Gal enzyme is encapsulated inside the vesicle by using an Alexa-647 labeled β-Gal (Figure 6b). To show that sequestered enzymes are still active and can be supplied with substrates from outside, we added 2 µL of fluorogenic substrate Fluorescein-di-beta-D-galactopyranoside (FDG, M_w = 657 Da) to the coacervate-core vesicles containing β-Gal. As shown in Figure 6c, we could observe clear fluorescence appearing inside the vesicles, and localizing in the shell region. This can be explained by the fact that FDG enters the coacervates from the outer solution through the semipermeable dityrosine membrane. Conversion will thus occur first at the boundary between the membrane and the coacervate core. Control experiments with empty CCVs and without substrate showed no significant fluorescence, (Figure 6d and Figure S17, Supporting Information) which confirms that the enzyme is encapsulated and active inside coacervate-core vesicles and that its substrate can diffuse through the membrane and reach the enzyme inside the coacervate protocells. These results show that tyrosine-containing peptide-based coacervates are promising compartments for encapsulation of active enzymes and other large molecules, which can be protected and retained by the oxidative
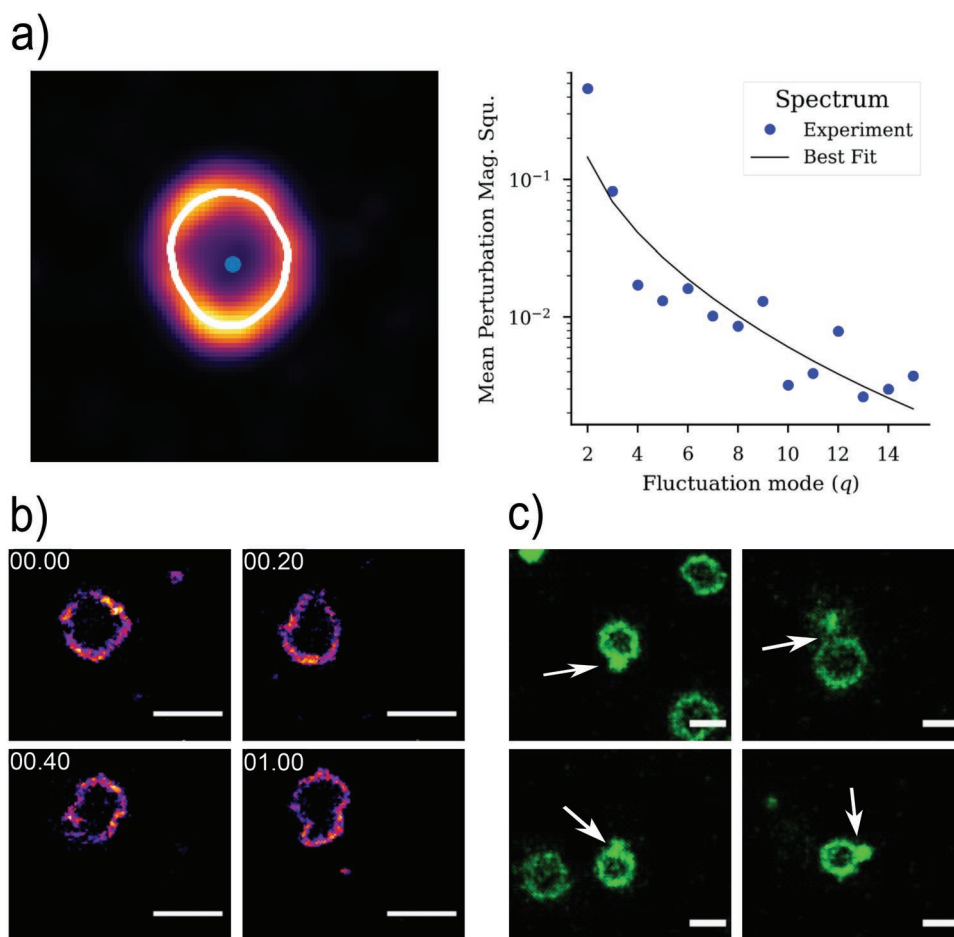
ADVANCED
SCIENCE NEWS
www.advancedsciencenews.com

ADVANCED
MATERIALS
www.advmat.de

Figure 5. Characterization of the membrane flexibility of CCVs. a) The processed image of a vesicle, with the surface outlined in white, calculated during the image-processing step of the flicker spectroscopy analysis (left). The intensity spectrum of the surface fluctuations is a function of Fourier mode (right). Blue dots: the fluctuations corrected for the possible nonspherical base shape of the CCVs. Black line: the best fit curve of the theoretical model to the corrected spectrum, which yields the estimates for surface tension and bending rigidity. b) Enhanced shape fluctuations of CCVs by increasing the pH after crosslinking (Video S4, Supporting Information). c) Shape fluctuations can result in the formation of buds at the surface of CCVs (Video S5, Supporting Information). Scale bars represent 3 μm in all images in (b) and (c).

assembly of a semipermeable membrane, and supplied with substrates and nutrients from the surrounding solution.

3. Conclusion

We report a new type of tyrosine-containing peptide conjugates that are able to undergo LLPS. Depending on the molecular characteristics of the spacer, the initial condensates can undergo rapid liquid-to-solid transition into needle-like fibers, a slow diffusion-limited agglomeration into fractals, or growth into large droplets by coalescence. The use of tyrosine residues makes these coacervate droplets responsive to alkaline conditions, which results in a well-defined pH window in which condensation occurs. We were able to crosslink the tyrosines at the coacervate surface by oxidation into semipermeable membranes with a thickness between 300–900 nm. The membrane is intrinsically fluorescent, and stabilizes the coacervate protocells against coalescence and ripening. Dispersions of coacervate-core vesicles can withstand centrifugation

and redispersion and they can be stored for more than a month, while unoxidized coacervates coalesce and settle in several hours. Despite its larger thickness, the dityrosine membrane resembles a phospholipid bilayer in terms of its bending rigidity (0.1 k_BT) and surface tension (45 nN m^{-1}), as determined by flicker spectroscopy. By slightly changing the volume of the coacervate core, deformations of the membrane can be enhanced to the point that buds are formed, which opens the way for fission of these hybrid protocells. The dityrosine-based membranes are significantly more permeable for small and polar molecules than phospholipid bilayers, readily taking up peptides like GSH and K_{10} and concentrating them tenfold. By analyzing the uptake as a function of probe molecular weight, we found an effective molecular weight cut-off of the membranes of 2.5 kDa. Finally, we demonstrated that these CCVs can be used to sequester and protect enzymes, and carry out reactions inside the vesicles on demand by supplying them with substrates from the outside solution. Taken together, these CCVs are promising hybrid protocell candidates, while their stability, intrinsic fluorescence and ability to
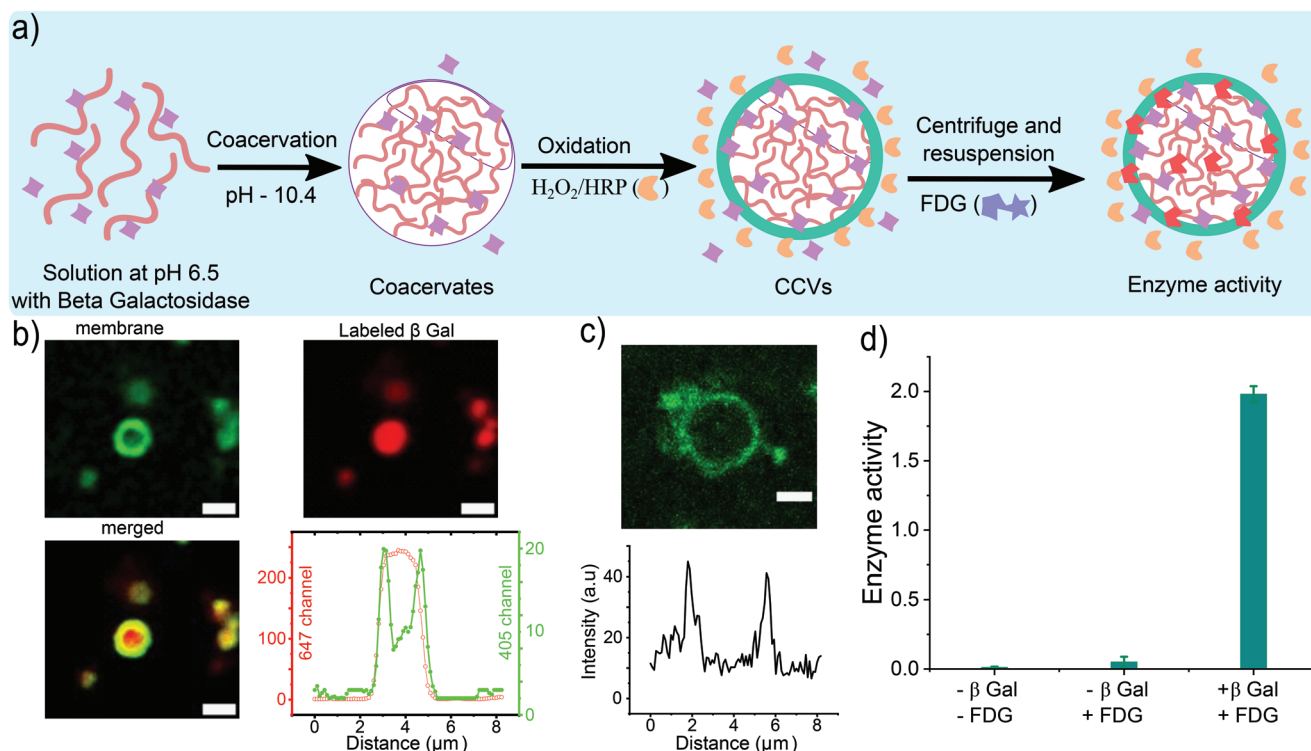
Figure 6. Enzymatic activity of β-Gal inside the CCVs and encapsulation ability of bigger molecular weight macromolecules. a) Schematic illustration of β-Gal encapsulation inside the CCVs, b) Alexa-647 labeled β-Gal encapsulated inside the coacervate-core vesicles, c) CCVs with encapsulated β-Gal after addition of the fluorogenic substrate FDG. d) β-Gal activity calculated from fluorescence signal of CCVs with encapsulated β-Gal ($n = 10$) and controls without encapsulated β-Gal or without FDG added. The scale bar in all images represents 2 μm.

sequester and maintain active enzymes make them also interesting for drug delivery applications.

4. Experimental Section

Synthesis of Peptide Derivatives: All peptide derivatives were synthesized in the laboratory by using standard solution phase peptide synthesis. Detailed procedures and characterization are provided in the Supporting information.

Preparation of Coacervates: The lyophilized powder of all peptide derivatives was dissolved in Milli-Q water (typically, 5 mg mL^{-1}), resulting in a clear solution with a pH $\approx$ 6. To induce phase separation, the pH was increased by addition of 1 μL of 1 M NaOH per mL solution. The solution became immediately turbid, and the formation of coacervates was confirmed by optical microscopy. Alternatively, coacervation was induced with Tris- buffer (100 $\times$ 10^{-3} M, pH 7.4) or phosphate buffer (100 $\times$ 10^{-3} M, pH 7.4) by mixing 1:1 with 2 mg mL^{-1} stock solution of the peptide derivatives. An Olympus optical microscope IX81 with an Orca Flash4.0 sCMOS camera was used to observe the coacervates in bright-field transmission or epifluorescence mode. The 5 μL turbid solution right after increasing the pH was placed on the cover glass with a thickness of 24 $\times$ 50 mm.

pH Window by Turbidity Measurements: The turbidity of coacervates was monitored by the Tecan Spark multimode plate reader with an in-built spectrophotometer. The detailed procedure is given in the Supporting Information.

Preparation of Semipermeable Coacervate-Core Vesicles: Coacervates of YFsFY and other derivatives were oxidized with horseradish peroxidase (HRP) in the presence of hydrogen peroxide (H$_2$O$_2$) to make semipermeable coacervate-core vesicles (CCVs). CCVs shown in

Figure 3 were prepared by using 400 μL containing YFsFY coacervates (concentration 10 mg mL^{-1}) at final pHs of 10–10.4, as measured by a pH meter and 40 μL H$_2$O$_2$ (1 M) was added and the sample was equilibrated for 1 min, and then 40 μL HRP (5 mg mL^{-1}) was added and the vial was kept at 4 °C for 24 h. CCVs presented in all other experiments were prepared from 5 mg mL^{-1} concentration of YFsFY coacervates: to 300 μL of coacervate dispersion at pH 10–10.5 we added 6 μL H$_2$O$_2$ (1 M), 18 μL HRP, mixed by mild vortexing and stored the reaction mixtures at 4 °C for 24 h. For effect of the concentration of oxidizing agent on the thickness of membrane (Figure S6, Supporting Information), 100 μL coacervates was used to prepare four different final concentration (3.7 $\times$ 10^{-3} M H$_2$O$_2$ and 0.056 mg mL^{-1} HRP), (18.5 $\times$ 10^{-3} M H$_2$O$_2$ and 0.28 mg mL^{-1} HRP), (46 $\times$ 10^{-3} M H$_2$O$_2$ and 0.56 mg mL^{-1} HRP), and (139 $\times$ 10^{-3} M H$_2$O$_2$ and 0.83 mg mL^{-1} HRP) of oxidizing agents. The result of the oxidation process was checked under the microscope after 24 h.

MALDI-TOF for Confirmation of Dityrosine: 100 μL YFsFY (3 mg mL^{-1}) was diluted in 900 μL Tris buffer (100 $\times$ 10^{-3} M, pH 9), which resulted in coacervates and 50 μL HRP (5 mg mL^{-1}) and 50 μL H$_2$O$_2$ were added to make the vesicles (24 h, 4 °C). After 24 h, the vesicles were freeze-dried to obtain a solid powder. Acetonitrile with 0.1% TFA was used to dissolve the oxidized YFsFY followed by 2 min of vortexing and 2 min of sonication. MALDI-TOF sample was prepared by 1:1 v/v with the MALDI matrix (α-cyano-4-hydroxycinnamic acid in 50% acetonitrile, 0.1% TFA in Milli-Q). The samples were dried in air and observed by MALDI-TOF.

Confocal Microscopy for the Encapsulation of Dyes: The permeability of fluorescent probe molecules into the coacervate-core vesicles was quantified by confocal fluorescence microscopy on a Leica Sp8x confocal microscope. The samples for confocal measurement were prepared by adding 1 μL of the stock solution containing the probe molecules into 50 μL volume (5 mg mL^{-1} YFsFY concentration) of coacervate-core vesicle dispersion. Concentration details of stock solutions of probe molecules are given in the Supporting information.

Flicker Spectroscopy Calculations: Time-series microscopy videos of thermally fluctuating coacervate-core vesicles were obtained as described above. Flicker spectroscopy was carried out as described in Law et al.[36] Briefly, the boundary of thermally fluctuating coacervate-core vesicles was extracted from confocal microscopy videos and the Fourier transform of this boundary was taken for each vesicle and averaged over time, yielding a fluctuation spectrum. A correction was made to account for the possible non-spherical base-shape.[33a] The resulting spectrum was fitted to the theoretical spectrum[37] which has two fitting parameters: surface tension and bending rigidity. The values reported in the text are the average and standard deviation of 10 analyzed time-series microscopy videos of thermally fluctuating coacervate-core vesicles.

Cleavage of a Substrate by the Enzyme: 10 μL of β-Gal 3 mg mL^{-1} was added to 250 μL of YFsFY solution at pH 6.5. The pH was increased to 10.4 by adding NaOH (1 M) to induce coacervation and subsequently 5 μL H$_2$O$_2$ (1 M) and 15 μL HRP (5 mg mL^{-1}) as oxidizing agents were used to make the vesicles. After 24 h, the coacervate-core vesicles were centrifuged at 4000 rcf for 5 min and supernatant was gently removed by pipetting, and the pellet was resuspended in the same volume of Milli-Q. 2 μL of the fluorogenic substrate fluorescein-di-beta-D-galactopyranoside (FDG) (15.4×10^{-3} M in DMSO) was added to 50 μL of fourfold diluted resuspended coacervate-core vesicles. The same concentration and volume of coacervate-core vesicles containing β-Gal was used for controls and the same FITC channel was used. Another control experiment was where the same volume and concentration of substrate was used in coacervate-core vesicles with no enzyme inside.

Supporting Information

Supporting Information is available from the Wiley Online Library or from the author.

Conflict of Interest

The authors declare no conflict of interest.

Author Contributions

M.A. and E.S. conceived and designed the project with input from W.T.S.H. M.A. carried out synthesis of derivatives and other microscopy experiments. J.O.L. and S.N.G. analyzed the membrane fluctuations by flicker spectroscopy. M.A. and E.S. wrote the manuscript with input from all co-authors.

Data Availability Statement

The data that support the findings of this study are available from the corresponding author upon reasonable request.

[1] N. A. Yewdall, A. F. Mason, J. C. M. van Hest, *Interface Focus* **2018**, *8*, 20180023.
[2] M. H. van Haren, K. K. Nakashima, E. Spruijt, *J. Syst. Chem.* **2020**, *8*, 107.
[3] M. Abbas, W. P. Lipiński, J. Wang, E. Spruijt, *Chem. Soc. Rev.* **2021**, *50*, 3690.
[4] a) A. F. Mason, J. C. M. van Hest, *Emerging Top. Life Sci.* **2019**, *3*, 567; b) Y. Zhang, Y. Chen, X. Yang, X. He, M. Li, S. Liu, K. Wang, J. Liu, S. Mann, *J. Am. Chem. Soc.* **2021**, *143*, 2866; c) K. K. Nakashima, M. A. Vibhute, E. Spruijt, *Front. Mol. Biosci.* **2019**, *6*, 21.
[5] a) F. Dyson, *Origins of life*, Cambridge University Press, Cambridge, UK **1999**; b) T. Z. Jia, C. Hentrich, J. W. Szostak, *Origins Life Evol. Biospheres* **2014**, *44*, 1.
[6] a) B. Mui, P. Cullis, E. Evans, T. Madden, *Biophys. J.* **1993**, *64*, 443; b) W.-C. Su, D. L. Gettel, M. Chabanon, P. Rangamani, A. N. Parikh, *J. Am. Chem. Soc.* **2018**, *140*, 691; c) T. F. Zhu, J. W. Szostak, *J. Syst. Chem.* **2011**, *2*, 4.
[7] a) T. D. Tang, C. R. C. Hak, A. J. Thompson, M. K. Kuimova, D. Williams, A. W. Perriman, S. Mann, *Nat. Chem.* **2014**, *6*, 527; b) F. P. Cakmak, A. M. Marianelli, C. D. Keating, *Langmuir* **2021**, *37*, 10366.
[8] A. F. Mason, B. C. Buddingh', D. S. Williams, J. C. M. van Hest, *J. Am. Chem. Soc.* **2017**, *139*, 17309.
[9] D. S. Williams, A. J. Patil, S. Mann, *Small* **2014**, *10*, 1830.
[10] N. N. Deng, W. T. S. Huck, *Angew. Chem., Int. Ed.* **2017**, *129*, 9868.
[11] N.-N. Deng, M. A. Vibhute, L. Zheng, H. Zhao, M. Yelleswarapu, W. T. S. Huck, *J. Am. Chem. Soc.* **2018**, *140*, 7399.
[12] S. Deshpande, F. Brandenburg, A. Lau, M. G. F. Last, W. K. Spoelstra, L. Reese, S. Wunnava, M. Dogterom, C. Dekker, *Nat. Commun.* **2019**, *10*, 1800.
[13] M. G. F. Last, S. Deshpande, C. Dekker, *ACS Nano* **2020**, *14*, 4487.
[14] C. Love, J. Steinkühler, D. T. Gonzales, N. Yandrapalli, T. Robinson, R. Dimova, T. Y. D. Tang, *Angew. Chem., Int. Ed.* **2020**, *59*, 5950.
[15] M. Abbas, W. P. Lipiński, K. K. Nakashima, W. T. S. Huck, E. Spruijt, *Nat. Chem.* **2021**, *13*, 1046.
[16] a) J. Wang, J.-M. Choi, A. S. Holehouse, H. O. Lee, X. Zhang, M. Jahnel, S. Maharana, R. Lemaitre, A. Pozniakovsky, D. Drechsel, *Cell* **2018**, *174*, 688; b) B. S. Schuster, G. L. Dignon, W. S. Tang, F. M. Kelley, A. K. Ranganath, C. N. Jahnke, A. G. Simpkins, R. M. Regy, D. A. Hammer, M. C. Good, *P. Natl. Acad. Sci. USA* **2020**, *117*, 11421; c) Y. Lin, S. L. Currie, M. K. Rosen, *J. Biol. Chem.* **2017**, *292*, 19110; d) B. Gabryelczyk, H. Cai, X. Shi, Y. Sun, P. J. Swinkels, S. Salentinig, K. Pervushin, A. Miserez, *Nat. Commun.* **2019**, *10*, 5465.
[17] W. C. Wimley, T. P. Creamer, S. H. White, *Biochemistry* **1996**, *35*, 5109.
[18] A. Patel, H. O. Lee, L. Jawerth, S. Maharana, M. Jahnel, M. Y. Hein, S. Stoynov, J. Mahamid, S. Saha, T. M. Franzmann, *Cell* **2015**, *162*, 1066.
[19] S. Koga, D. S. Williams, A. W. Perriman, S. Mann, *Nat. Chem.* **2011**, *3*, 720.
[20] B. Gabryelczyk, H. Cai, X. Shi, Y. Sun, P. J. M. Swinkels, S. Salentinig, K. Pervushin, A. Miserez, *Nat. Commun.* **2019**, *10*, 5465.
[21] K. K. Nakashima, M. H. I. van Haren, A. A. M. André, I. Robu, E. Spruijt, *Nat. Commun.* **2021**, *12*, 3819.
[22] G. R. Grimsley, J. M. Scholtz, C. N. Pace, *Protein Sci.* **2009**, *18*, 247.

**ADVANCED
SCIENCE NEWS**

www.advancedsciencenews.com

**ADVANCED
MATERIALS**

www.advmat.de

[23] a) Y. K. Al-Hilaly, L. Biasetti, B. J. Blakeman, S. J. Pollack, S. Zibaee, A. Abdul-Sada, J. R. Thorpe, W.-F. Xue, L. C. Serpell, *Sci Rep* **2016**, *6*, 39171; b) D. Balasubramanian, R. Kanwar, *Oxygen/Nitrogen Radicals: Cell Injury and Disease*, Springer, New York **2002**, p. 27.

[24] a) X. Ren, Q. Zou, C. Yuan, R. Chang, R. Xing, X. Yan, *Angew. Chem., Int. Ed.* **2019**, *131*, 5930; b) J. Lee, M. Ju, O. H. Cho, Y. Kim, K. T. Nam, *Adv. Sci.* **2019**, *6*, 1801255; c) A. Lampel, S. A. McPhee, H.-A. Park, G. G. Scott, S. Humagain, D. R. Hekstra, B. Yoo, P. W. Frederix, T.-D. Li, R. R. Abzalimov, S. G. Greenbaum, T. Tuttle, C. Hu, C. J Bettinger, R. V. Ulijn, *Science* **2017**, *356*, 1064.

[25] K. I. Min, D. H. Kim, H. J. Lee, L. Lin, D. P. Kim, *Angew. Chem., Int. Ed.* **2018**, *130*, 5732.

[26] a) C. Wanzke, A. Jussupow, F. Kohler, H. Dietz, V. R. I. Kaila, J. Boekhoven, *ChemSystemsChem* **2020**, *2*, 1900044; b) K. K. Nakashima, J. F. Baaij, E. Spruijt, *Soft Matter* **2018**, *14*, 361.

[27] a) X. Huang, M. Li, D. C. Green, D. S. Williams, A. J. Patil, S. Mann, *Nat. Commun.* **2013**, *4*, 2239; b) A. Joesaar, S. Yang, B. Bögels, A. van der Linden, P. Pieters, B. Kumar, N. Dalchau, A. Phillips, S. Mann, T. F. de Greef, *Nat. Nanotechnol.* **2019**, *14*, 369; c) P. Zhou, X. Liu, G. Wu, P. Wen, L. Wang, Y. Huang, X. Huang, *ACS Macro Lett.* **2016**, *5*, 961; d) W. Mu, Z. Ji, M. Zhou, J. Wu, Y. Lin, Y. Qiao, *Sci. Adv.* **2021**, *7*, eabf9000.

[28] a) A. Dinsmore, M. F. Hsu, M. Nikolaides, M. Marquez, A. Bausch, D. Weitz, *Science* **2002**, *298*, 1006; b) M. Li, R. L. Harbron, J. V. Weaver, B. P. Binks, S. Mann, *Nat. Chem.* **2013**, *5*, 529; c) J.-W. Kim, A. Fernández-Nieves, N. Dan, A. S. Utada, M. Marquez, D. A. Weitz, *Nano Lett.* **2007**, *7*, 2876; d) C. Wu, S. Bai, M. B. Ansorge-Schumacher, D. Wang, *Adv Mater* **2011**, *23*, 5694; e) H. Wu, X. Du, X. Meng, D. Qiu, Y. Qiao, *Nat. Commun.* **2021**, *12*, 6113.

[29] a) J. Daillant, E. Bellet-Amalric, A. Braslau, T. Charitat, G. Fragneto, F. Graner, S. Mora, F. Rieutord, B. Stidder, *P. Natl. Acad. Sci. USA* **2005**, *102*, 11639; b) P. Bassereau, P. Sens, *Physics of Biological Membranes*, Springer, New York **2018**. c) R. Lipowsky, *J. Biol. Chem.* **2014**, *395*, 253.

[30] R. Lipowsky, *Adv. Colloid Interface Sci.* **2014**, *208*, 14.

[31] G. Brannigan, F. L. Brown, *Biophys. J.* **2006**, *90*, 1501.

[32] J. El-Beyrouthy, M. M. Makhoul-Mansour, G. Taylor, S. A. Sarles, E. C. Freeman, *J. R. Soc. Interface* **2019**, *16*, 20190652.

[33] a) J. Pécréaux, H. G. Döbereiner, J. Prost, J. F. Joanny, P. Bassereau, *Eur. Phys. J. E* **2004**, *13*, 277; b) R. Dimova, *Adv. Colloid Interface Sci.* **2014**, *208*, 225.

[34] a) M. Simunovic, C. Prévost, A. Callan-Jones, P. Bassereau, *Philos. Trans. R. Soc. A* **2016**, *374*, 20160034; b) M. Simunovic, J.-B. Manneville, H.-F. Renard, E. Evergren, K. Raghunathan, D. Bhatia, A. K. Kenworthy, G. A. Voth, J. Prost, H. T. McMahon, *Cell* **2017**, *170*, 172.

[35] M. Matsuo, K. Kurihara, *Nat. Commun.* **2021**, *12*, 5487.

[36] J. O. Law, C. M. Jones, T. Stevenson, M. S. Turner, H. Kusumaatmaja, S. N. Grellscheid, *bioRxiv* **2022**, https://doi.org/10.1101/2022.05.03.490456.

[37] W. Häckl, U. Seifert, E. Sackmann, *J. Phys. II France* **1997**, *7*, 1141.